Journal of Vacuum Science and Technology A

RESEARCH ARTICLE | FEBRUARY 13 2025

In situ growth of ultrathin Y_2O_3 capping layers for Eu-organic thin films via atomic/molecular layer deposition

Special Collection: Atomic Layer Deposition (ALD)

Topias Jussila ; Joona Pekkanen ; Anni Virta ; Amr Ghazy ; Mika Lastusaari ;
Maarit Karppinen

J. Vac. Sci. Technol. A 43, 022406 (2025)
https://doi.org/10.1116/6.0004237

Articles You May Be Interested In

Low-pressure thermogravimetric analysis for finding sublimation temperatures for organic precursors in atomic/molecular layer deposition

J. Vac. Sci. Technol. A (August 2020)

Gas phase growth of metal-organic frameworks on microcantilevers for highly sensitive detection of volatile organic compounds

APL Mater. (June 2024)

Recent trends in thermal atomic layer deposition chemistry

J. Vac. Sci. Technol. A (March 2025)

04 April 2025 08:29:42

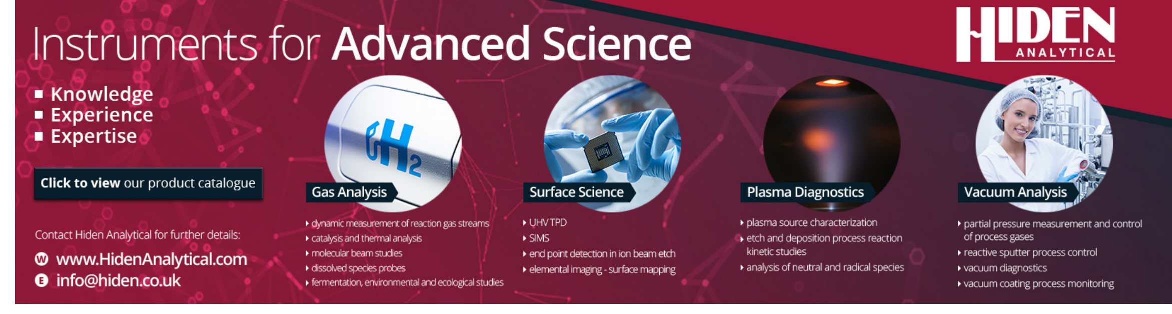

JVST A
Journal of Vacuum Science & Technology A
ARTICLE
pubs.aip.org/avs/jva

In situ growth of ultrathin Y_2O_3 capping layers for Eu-organic thin films via atomic/molecular layer deposition

Cite as: J. Vac. Sci. Technol. A **43**, 022406 (2025); doi: 10.1116/6.0004237
Submitted: 26 November 2024 · Accepted: 29 January 2025 ·
Published Online: 13 February 2025

Topias Jussila,[1] Joona Pekkanen,[1] Anni Virta,[1] Amr Ghazy,[1] Mika Lastusaari,[2] and Maarit Karppinen[1,a)]

AFFILIATIONS

[1]Department of Chemistry and Materials Science, Aalto University, Aalto FI-00076, Finland
[2]Department of Chemistry, University of Turku, Turku FI-20014, Finland

Note: This paper is part of the 2025 Special Topic Collection on Atomic Layer Deposition (ALD).
[a)]**Author to whom correspondence should be addressed:** maarit.karppinen@aalto.fi

ABSTRACT

Metal-organic thin films fabricated through industry-feasible atomic/molecular layer deposition (ALD/MLD) routes are highly attractive materials with diverse functional properties, but they suffer from poor chemical stability in ambient (humid) conditions and especially in direct contact with liquids which limits their practical implementation. The most efficient way to protect the inherently unstable thin films is to encapsulate them with chemically inert material layers without exposing the metal-organic material to air during the processing. Here, we demonstrate the robust *in situ* encapsulation of luminescent ALD/MLD-grown Eu-organic (europium hydroxyquinoline carboxylate) thin films with ultrathin (1–12 nm) ALD-grown Y_2O_3 capping layers deposited under the same deposition conditions. From x-ray reflectivity analysis, the successful capping-layer formation with only a minor etching effect on the underlining Eu-organic film was confirmed despite the use of the strongly oxidizing reactant (O_3) for the ALD Y_2O_3 process. Importantly, the film composition and luminescent properties were not compromised by the etching. The stability of the encapsulated thin films was studied in both dry and humid air, as well as in liquid water. The results revealed that already a 3–4 nm Y_2O_3 capping layer effectively increases the Eu-organic film stability both when stored in open air and when exposed to liquid water. The enhanced stability in the liquid environment is, in particular, critical for the use of Eu-organic thin films for bioimaging applications.

© 2025 Author(s). All article content, except where otherwise noted, is licensed under a Creative Commons Attribution-NonCommercial 4.0 International (CC BY-NC) license (https://creativecommons.org/licenses/by-nc/4.0/). https://doi.org/10.1116/6.0004237

04 April 2025 08:29:42

I. INTRODUCTION

Metal-organic thin films are expected to have a major impact on various technologies including sensing, energy storage, and catalysis;[1,2] the seemingly endless collection of organic molecules (aliphatic and aromatic alcohols, amines, carboxylic acids, thiols, etc.) which can form continuous networks with inorganic units (atoms or clusters) offer vast possibilities in structure, porosity, and functional property engineering.[3–5] However, the major concern regarding the metal-organic thin films—which is likely to limit their practical implementation—is the poor chemical stability. The organic species and especially the bonding groups between the metal (M) and organic (R) species (e.g., R-O-M-O-R or R-N-M-N-R) are often air-sensitive and readily cleaved in the presence of water vapor.[6] Hence, it is most important to develop efficient industry-feasible strategies to protect these inherently air-sensitive materials from the chemical decomposition without compromising their functional properties. The most efficient route would be to encapsulate the metal-organic film with a thin, chemically inert, inorganic metal oxide capping layer through an *in situ* deposition process. This requires compatible processes for both the material types.

Among various fabrication routes,[7] atomic/molecular layer deposition (ALD/MLD) is a leading gas-phase and solvent-free deposition technique of advanced metal-organic thin films.[8] It

provides unique advantages such as molecular scale film thickness control as well as excellent uniformity and conformality even on high-aspect-ratio structures. The two deposition methods, i.e., the already widely industry-implemented ALD technique for inorganics and its newer counterpart MLD for organics, are both based on self-terminating gas-surface reactions between sequentially introduced vaporized precursors separated by inert gas purging. This unique precursor feeding scheme enables the highly controlled film growth. While the combined ALD/MLD technique is used to obtain the functional metal-organic thin film, the ALD technique is most attractive for the encapsulation of the metal-organic thin film due to its superior ability to yield pinhole-free layers with ultrathin thicknesses.[9] The capping layer should be sufficiently thin not to dampen the functional properties of the metal-organic film or the targeted device.[10] Most importantly, ALD/MLD and ALD have similar working principles and reactor/deposition conditions and are, thus, a prime combination for *in situ* deposition of metal-organic/metal oxide dual-layer structures.[11]

The capping layer approach is a well-known concept to increase the chemical stability and lifetime of organic-based thin-film materials and devices.[12,13] In particular, ALD-grown metal oxide coatings have been frequently employed to encapsulate organic light emitting diodes,[12,14,15] organic solar cells,[16–18] and organic field-effect transistors.[19] In most of the studies, the well-established ALD Al_2O_3 process has been used owing to its robustness and the relatively good barrier properties of ultrathin amorphous Al_2O_3 coatings. The Al_2O_3 layer has been also mixed with other oxide (i.e., ZrO_2 or HfO_2) layers for improved stability and gas barrier performance.[20–22] On the other hand, for the encapsulation of metal-organic thin films grown with ALD/MLD, very limited research has been performed. The few examples include the encapsulation of ALD/MLD alucone (Al + diethylene glycol) thin films with Al_2O_3; here, the ALD coating improved the extremely poor air-stability of the alucone films significantly.[23] The ALD/MLD and ALD techniques have also been employed for the growth of inorganic-organic nanolaminates (e.g., Al_2O_3/alucone)[24] for improved mechanical properties and device stability.[25–28]

Apart from the air-stability, many practical applications operate in more severe chemical environments such as aqueous solutions. Metal-organic thin-film materials are usually unstable in such conditions which imposes restrictions for applications intended to operate in conditions beyond open air. We recently reported an ALD/MLD process for novel luminescent Eu-HQA (HQA: 2-hydroxyquinoline-4-carboxylic acid) thin films that could potentially be applied for advanced Förster resonance energy transfer (FRET) based bioimaging devices owing to the appreciably wide excitation wavelength band (up to 400 nm in the visible light region) of the HQA molecule.[10] However, the Eu-HQA films dissolve nearly immediately in the fluorescent dyes employed in the imaging procedure which precludes the imaging in practice. To address this issue, we report here a new *in situ* encapsulation process for Eu-HQA films. The process consists of the ALD/MLD growth of the Eu-HQA layer from Eu(thd)$_3$ (thd = 2,2,6,6-tetramethyl-3,5-heptanedione) + HQA precursors, followed by ALD growth of ultrathin (1–12 nm) Y_2O_3 capping layer under the same deposition conditions. The thickness range of the capping layer was selected based on the targeted bioimaging application which limits the capping-layer thickness to ∼10 nm in maximum.[29] The motivation to select Y_2O_3 as the capping-layer material was threefold: (i) our interest to expand the very limited repertoire of ALD encapsulation processes, (ii) the excellent temperature compatibility of the two processes, Y(thd)$_3$ + O_3 and Eu(thd)$_3$ + HQA, and (iii) the apparent ease to dope Y_2O_3 films with lanthanide activators for enhanced overall luminescence output,[30,31] to be challenged in future studies.

The present Eu-HQA and Eu-HQA/Y_2O_3 thin films are characterized using x-ray reflectivity (XRR) which is a precise and time-efficient technique to estimate thin films and multilayer structures without the need for demanding and time-consuming cross-sectional electron microscopy imaging. The capping performance of the Y_2O_3 layer is studied in three different chemical environments, dry and humid air, and liquid water, using XRR and FTIR (Fourier transform infrared spectroscopy) measurements. Most importantly, our results demonstrate the significantly improved stability of the Eu-HQA/Y_2O_3 films in liquid water. In a broader scope, this study opens new prospects for the application space of ALD/MLD-grown metal-organic thin films by reporting an industry-relevant one-process-step encapsulation approach to enhance the often distinguishably poor water/humidity resistance of these otherwise extremely attractive functional thin-film materials.

II. EXPERIMENT

A flow-type hot-wall ALD reactor (F-120 by ASM Microchemistry Ltd.) was employed to deposit the Eu-HQA, Y_2O_3, and Eu-HQA/Y_2O_3 films. The Eu-HQA films were deposited using in-house synthesized Eu(thd)$_3$,[32] and commercial HQA (Sigma Aldrich, 97%) precursors, with sublimation temperatures of 140 and 210 °C, respectively. For the Y_2O_3 films, in-house synthesized Y(thd)$_3$ at sublimation temperature of 130 °C and ozone (O_3), generated with Triogen Lab2b ozone generator from oxygen gas (≥99%), were used as the precursors. The metal and organic precursors were placed in open glass crucibles inside the reactor. The reactor pressure was kept at ∼4 mbar and nitrogen (N_2, 99.999%) was used as the purging and carrier gas. The deposition temperature was kept at 250 °C for all depositions, and the films were deposited on ∼$2 \times 2\ cm^2$ Si(100) substrates (Okmetic Ltd.) with a native oxide layer.

Based on our previous report,[10] the precursor/purge lengths for the Eu-HQA deposition were fixed as follows: 4 s Eu(thd)$_3$/6 s N_2 purge/4 s HQA/6 s N_2 purge. For the Y_2O_3 deposition, the sequence was set to 4 s Y(thd)$_3$/4 s N_2 purge/3 s O_3/6 s N_2 purge.[33] The same precursor pulse and purge lengths were applied for the dual-layer Eu-HQA/Y_2O_3 film depositions.

Both the single and the dual-layer films were measured with XRR (PANalytical X'Pert Pro, Cu-Kα radiation), and the measured XRR curves were fitted using X'Pert Reflectivity software (PANalytical) to determine the film thickness, density, and roughness values. The surface morphology of the films was studied with atomic force microscopy (AFM; Bruker Dimension Icon AFM) on $2 \times 2\ \mu m^2$ area using ScanAsyst imaging mode, 1 Hz scan rate, and 512 × 512 pixels scan resolution. FTIR (Bruker alpha II) was used in the transmission mode to characterize the chemical composition of the films across the range of 400–4000 cm^{-1}. The FTIR signal from the Si substrate was subtracted from the sample data.

04 April 2025 08:29:42

© Author(s) 2025

Luminescence excitation and emission spectra were measured at room temperature using an Edinburgh Instruments FLS1000 spectrometer equipped with a continuous wave 450 W Xe arc lamp and PMT-900 photomultiplier tube. The spectra are corrected for the sensitivity of the setup at different wavelengths.

The XRR and FTIR techniques were used to evaluate the film stability under dry (20% relative humidity) and humid (80% relative humidity) conditions at room temperature (22 °C). To assess the stability of the Eu-HQA/Y_2O_3 dual-layer films in aqueous environments, water stability tests were performed under UV-light ($\lambda = 365$ nm) with different Y_2O_3 barrier layer thicknesses. A water droplet was placed on the sample surface under the UV-illumination, and the time for the luminescence to disappear (film decomposition) was monitored by eye.

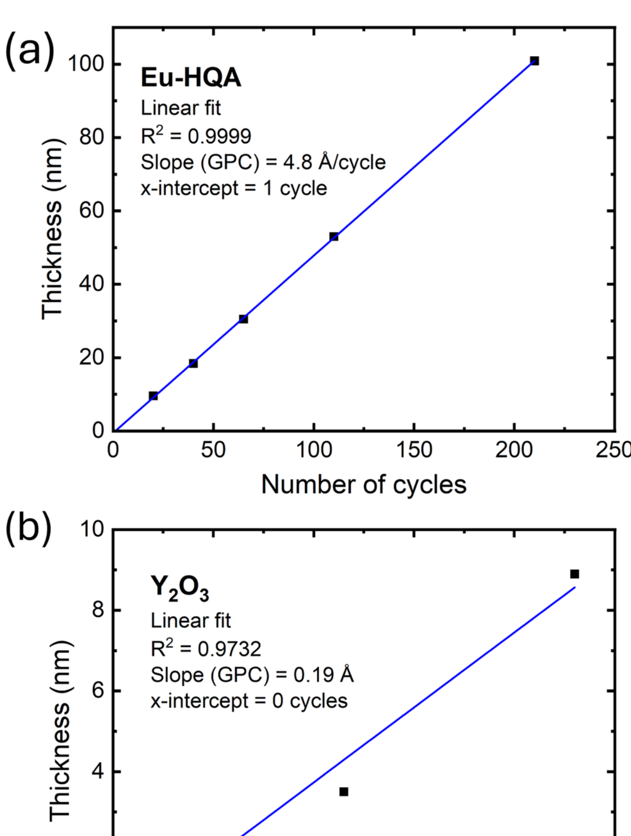

FIG. 1. Film thickness vs number of cycles for (a) Eu-HQA and (b) Y_2O_3 thin films grown on Si(100) substrates. The blue lines are the linear fittings of the data points.

III. RESULTS AND DISCUSSION

A. Atomic/molecular layer deposition

The binary processes for the Eu-HQA and Y_2O_3 single-layer films were established on Si(100) substrates prior to the Eu-HQA/Y_2O_3 dual-layer depositions. The ALD/MLD process for the Eu-HQA films was optimized in our previous report,[10] and the same precursor pulsing and purging recipe was applied here. However, the deposition temperature was set slightly higher (250 °C) compared to the original report (210–240 °C) since this was found to yield the best compatibility with the Y_2O_3 process in preliminary testing. The Eu-HQA process was confirmed to be perfectly linear regarding the film thickness versus number of ALD/MLD cycles applied at 250 °C; from the slope, the growth-per-cycle (GPC) value was determined to be 4.8 Å [Fig. 1(a)]. This is in line with the GPC trend previously observed for the $Eu(thd)_3$ + HQA process in the 210–240 °C range, showing a decrease of the GPC from 7.3 to 5.5 Å with increasing temperature. For the Y_2O_3 ALD process, the precursor pulsing and purging scheme was also adapted from the literature.[33] The obtained GPC of 0.19 Å [Fig. 1(b)] was rather low but close to the previously reported value (0.23 Å).[33] The small difference could be due to small differences in O_3 concentration (dose) and/or deposition temperature.

The two binary processes were employed as such for the *in situ* growth of the Eu-HQA/Y_2O_3 dual-layer films on the Si(100) substrates. The thickness of the Eu-HQA layer was fixed to 20 nm while the thickness of the Y_2O_3 capping layer was varied between 0.75 and 12.0 nm. Figure 2 shows the XRR patterns for the Eu-HQA/Y_2O_3 thin films. In XRR, the oscillation frequency

04 April 2025 08:29:42

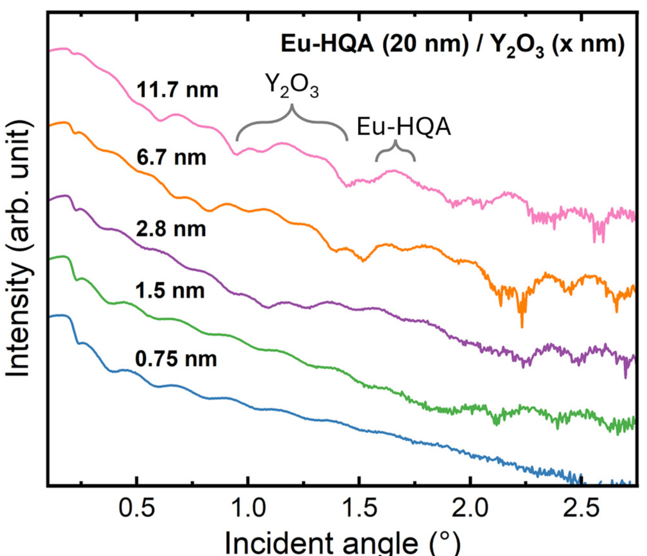

FIG. 2. XRR patterns for the Eu-HQA/Y_2O_3 dual-layer thin films grown on Si (100) substrates. Thickness of the Eu-HQA layer is 20 nm while the Y_2O_3 layer varies between 0.75 and 12 nm. The shown thicknesses are the aimed values for the Y_2O_3 layers based on the GPC (0.19 Å) of the Y_2O_3 ALD process.

© Author(s) 2025

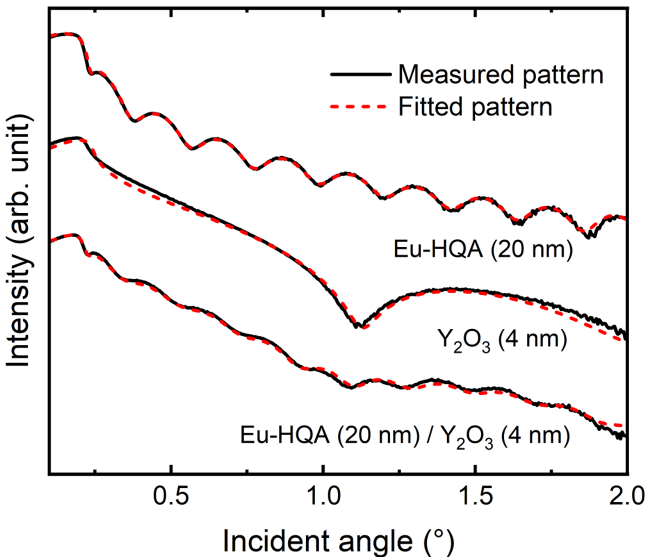

FIG. 3. Measured (black line) and fitted (red dashed line) XRR patterns for Eu-HQA (20 nm), Y_2O_3 (4 nm), and Eu-HQA (20 nm)/Y_2O_3 (4 nm) thin films.

depends on the layer thickness such that the higher the frequency (i.e., the shorter the oscillation length or so-called Kiessig fringes), the thicker the layer. The measured XRR patterns in Fig. 2 are the sum of two different oscillation frequencies which denotes the dual-layer structures. The smaller Eu-HQA Kiessig fringes remain the same for each sample which indicates the constant layer thickness as designed. On the other hand, the larger Y_2O_3 Kiessig fringes get expectedly smaller when the thickness of the Y_2O_3 layer is increased. Note that the Y_2O_3 contribution is difficult to distinguish for the Eu-HQA (20 nm)/Y_2O_3 (0.75 nm) film due to the extremely thin Y_2O_3 layer and, thus, broad Kiessig fringes.

For quantitative analyses, full fittings of the XRR patterns were performed to properly evaluate the feasibility of the depositions and to obtain the layer thickness, density, and roughness values. Figure 3 shows the measured (black line) and fitted XRR patterns (red dashed line) for single-layer Eu-HQA (20 nm) and Y_2O_3 (4 nm) films and for the Eu-HQA (20 nm)/Y_2O_3 (4 nm) dual-layer film. For the single-layer Eu-HQA film, the fitting model to describe the full sample was Si/SiO_2/Eu-HQA. The extracted density and root-mean-square roughness values were 2.0 g/cm^3 and 0.4 nm, respectively. The density of the Eu-HQA film is in the same range as for other ALD/MLD-grown lanthanide-organic thin films,[34,35] whereas the low roughness (<1 nm) is expected from an amorphous ALD/MLD-grown film.[36–38] For the 4-nm Y_2O_3 film, the fitting model was Si/SiO_2/Y_2O_3, and the extracted density and roughness were 4.4 g/cm^3 and 0.7 nm, respectively. The density of the Y_2O_3 film is lower than the ideal density of crystalline bulk Y_2O_3 (5.0 g/cm^3). The oxide films were x-ray amorphous and hence the relatively low density is reasonable as an amorphous phase typically has a lower density compared to a crystalline (close-packed) structure. Moreover, thin films often have different densities from the bulk, especially with ultralow thicknesses due to interface effects.[39,40]

For the Eu-HQA/Y_2O_3 dual-layer films, the best XRR fit was achieved with the following model: Si/SiO_2/Eu-HQA/Y_2O_3. The fitting results for the dual-layer films shown in Fig. 2 are listed in Table I. The extracted thickness values present minor deviations compared to the single-layer films. The GPC of the Y_2O_3 capping layer decreases gradually with increasing Y_2O_3 layer thickness: the GPC (0.34–0.28 Å) is relatively high for the thinnest Y_2O_3 layers (1–2 nm) and then decreases toward the average GPC value seen for the Y_2O_3 ALD process (0.19 Å) for the thicker (6–9 nm) Y_2O_3 capping layers. Several factors such as infiltration or enhanced nucleation may cause this trend. The gaseous Y(thd)$_3$ precursor molecules may partially infiltrate into the low-density Eu-HQA layer which would result in gas-phase reactions, and, thus, higher growth rate, due to prolonged evacuation of the infiltrated species.[41] On the other hand, the Y(thd)$_3$ molecules may nucleate more efficiently on the Eu-HQA surface with different active sites (COOH, OH, NH) compared to the Si/SiO_2 (with OH sites) or the Y_2O_3 surface.

For the Eu-HQA layer, the thickness is around 17–18 nm for all samples which is slightly lower than the target thickness (20 nm). We attribute this to a minor etching of the Eu-HQA layer due to O_3 exposure. The etching is expected to occur only during the initial Y(thd)$_3$ + O_3 ALD cycles, i.e., when the Eu-HQA layer is directly exposed to the O_3 gas. Once the Eu-HQA layer is protected

04 April 2025 08:29:42

TABLE I. Layer thickness, density, and roughness values for the Eu-HQA/Y_2O_3 dual-layer films from XRR fittings. The employed fitting model was Si/SiO_2/Eu-HQA/Y_2O_3.

Aimed thicknesses Eu-HQA + Y_2O_3 (nm)	Layer	Thickness (nm)	Density (g/cm^3)	Roughness (nm)
20 + 0.75	Y_2O_3	1.4	4.0	0.6
	Eu-HQA	17.4	1.9	0.5
20 + 1.5	Y_2O_3	2.3	4.1	0.6
	Eu-HQA	16.8	2.0	0.6
20 + 2.8	Y_2O_3	4.3	4.1	0.5
	Eu-HQA	17.9	2.1	0.6
20 + 6.7	Y_2O_3	6.2	4.3	0.5
	Eu-HQA	18.2	2.1	0.5
20 + 11.7	Y_2O_3	9.2	4.3	0.6
	Eu-HQA	17.3	2.1	0.6

© Author(s) 2025

by the formed Y_2O_3 layer, additional $Y(thd)_3 + O_3$ cycles will not cause any further etching. Based on the constant Eu-HQA layer thickness (within experimental accuracy) for all the dual-layer films in Table I, we assume that a sufficient protection is achieved already during the growth of the thinnest Y_2O_3 capping layer (1.4 nm) which corresponds to 40 ALD Y_2O_3 cycles.

We verified the suspected etching effect by exposing the Eu-HQA film to a prolonged O_3 vapor directly after the deposition which resulted in essentially complete etch of the film. Seemingly, the organic etching products were volatile as nothing was observed (XRR or FTIR) on the fully etched Eu-HQA film. No traces of EuO_x from the etching were observed due to the low remaining material amount and weak IR activity of metal oxides.

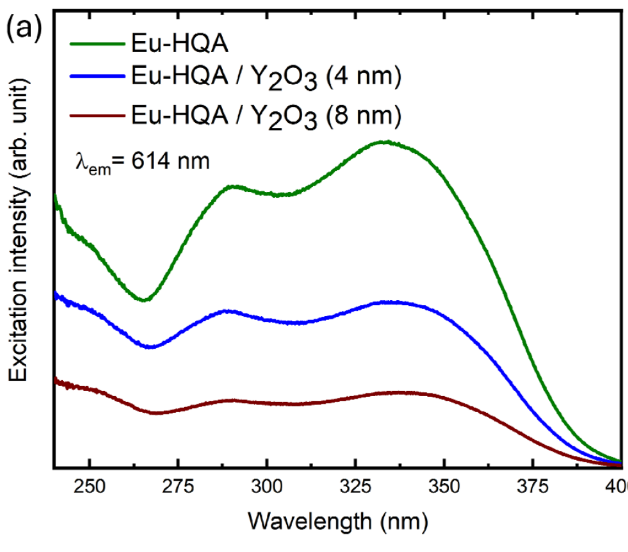

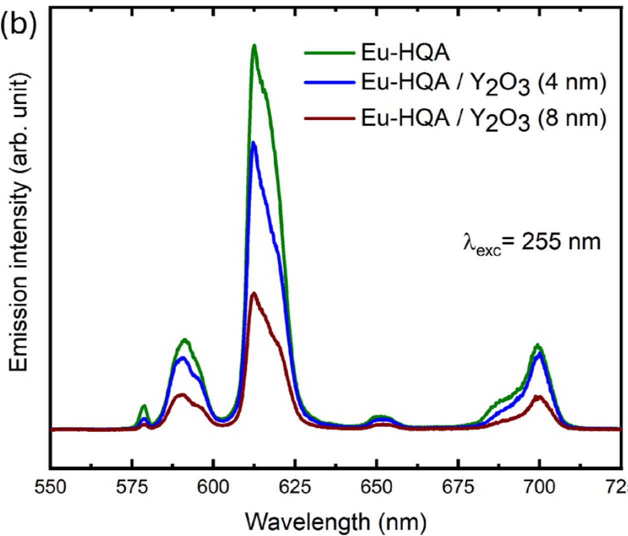

FIG. 4. (a) Excitation and (b) emission spectra of Eu-HQA single-layer and Eu-HQA/Y_2O_3 dual-layer films with 4 and 8 nm capping-layer thicknesses. The thickness of the Eu-HQA layer is 50 nm for each sample.

Most importantly, the minor etching (~2 nm) of the Eu-HQA layer during the Eu-HQA/Y_2O_3 deposition does not affect notably the functional properties of the films. Figure 4 shows both the excitation and emission spectra for an Eu-HQA (50 nm) single-layer and Eu-HQA (50 nm)/Y_2O_3 (4 or 8 nm) dual-layer films. For all the samples, both the excitation [Fig. 4(a)] and emission [Fig. 4(b)] wavelengths stay characteristic for the Eu-HQA thin films with the main red Eu^{3+} emission peak at 615 nm.[10] The decrease in the intensities is attributed mainly to the Y_2O_3 layer thickness since the etched Eu-HQA layer thickness is the same irrespective of the Y_2O_3 layer thickness (Table I) and yet the excitation and emission intensities clearly decrease with the increasing Y_2O_3 layer thickness. This issue could be mitigated through different strategies. First, Y_2O_3 serves as an excellent host matrix for lanthanide activators and could be doped with Eu for luminescent Eu:Y_2O_3 layers to enhance the overall luminescence intensity of the film.[30] Second, a three dimensional nanoplasmonic substrate can enhance the intensity by orders of magnitude and, thus, alleviate the shielding effect of the capping layer.[10] Furthermore, to avoid the etching effect of O_3, the $Y(thd)_3$ precursor with a strong metal-ligand bonding and, thus, low reactivity could be replaced with a more reactive yttrium precursor (e.g., yttrium acetamidinates) which do not require O_3 as the coreactant.[42]

Interestingly, we noticed that the etching effect became significant only if the Y_2O_3 layer was not applied immediately after the Eu-HQA deposition; we demonstrated this by applying a waiting time of 5 h between the growth of the Eu-HQA and Y_2O_3 layers. Apparently, the Eu-HQA surface is passivated during the elongated idle time in the reactor conditions (250 °C, N_2, ~4 mbar) such that it prevents the efficient $Y(thd)_3$ nucleation, thus allowing the more severe etching effect during the ozone pulse on the underlying metal-organic film. Further studies are required to reveal the mechanism and rate of passivation.

04 April 2025 08:29:42

The XRR-simulated density (1.9–2.1 g/cm^3) and roughness (0.5–0.6 nm) values of the Eu-HQA layer in the double-layer films are very close to the single-layer values (2.0 g/cm^3 and 0.4 nm). For the Y_2O_3 layer in the Eu-HQA/Y_2O_3 films, the roughness values observed (0.5–0.6 nm) are similar to the single-layer value (0.7 nm) but the density seems to increase with the increasing Y_2O_3 layer thickness: for the thinnest Y_2O_3 capping layers (<3 nm), the density is low (4 g/cm^3) but reaches a value of 4.3 g/cm^3 for 7 nm thick layers which is close to the pure Y_2O_3 film value (4.4 g/cm^3). It seems the Y_2O_3 film reaches the bulk-phase nature only after a certain threshold thickness (few nm) when grown on the low-density metal-organic layer.

Surface morphology of the films was also studied via AFM (supplementary material). For both the Eu-HQA single-layer and Eu-HQA/Y_2O_3 dual-layer thin films, the obtained surface roughness values were found to be in very good agreement with those determined from the XRR data. The surface roughness increases negligibly from 0.3 nm (single-layer Eu-HQA) to 0.5 nm (dual-layer Eu-HQA/Y_2O_3) despite the etching during the Y_2O_3 process. Additionally, the Y_2O_3 capping layer seems to slightly affect the surface morphology toward more distinct particlelike surfaces compared to the cap-less Eu-HQA sample.

© Author(s) 2025

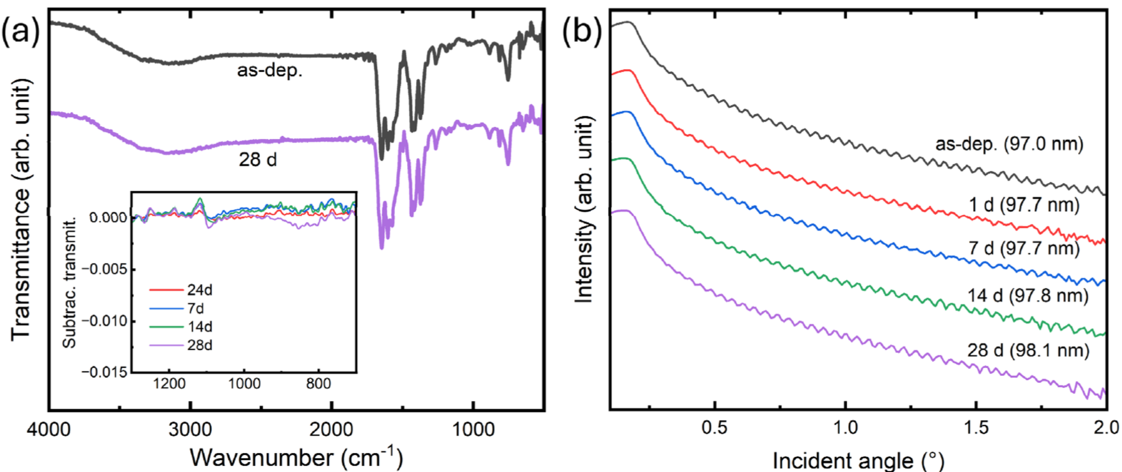

FIG. 5. (a) FTIR spectra and (b) XRR patterns for Eu-HQA thin films with indicated storage times in dry air (20% relative humidity at 22 °C). The inset in (a) shows the residual plots after subtracting the as-deposited sample spectrum from the aged samples with indicated storage times.

B. Film stability

The Eu-HQA and Eu-HQA/Y_2O_3 films were stored in both dry and humid air to study the stability of Eu-HQA toward oxygen and water vapor and the effect of the capping layer on the film stability. Figure 5 shows the FTIR spectra and XRR patterns for a cap-less Eu-HQA film stored in dry (relative humidity level 20%) air. The as-deposited (0 d storage time) FTIR spectrum is similar to our original report[10] showing that all the reactive groups (—COOH, —NH, —OH, ═O) of the HQA precursor have reacted nearly completely with the Eu(thd)$_3$ precursor as no IR signals can be seen around 1700 cm^{-1} (—COOH, ═O) or 2200–2900 cm^{-1} (—NH, —OH). The broad but weak signal around 2800–3700 cm^{-1} could be from both C—H stretching of the organics ring structures and some nonreacted —NH and —OH groups of the HQA precursor. Moreover, the characteristic signal of the thd-ligands at 2950 cm^{-1} cannot be observed. Most notably, the Eu-HQA films have excellent chemical stability in the dry air as no changes can be observed for the FTIR spectra with the sample storage time up to 28 days. The inset in Fig. 5(a) shows the residual plots in the IR fingerprint area (1300–700 cm^{-1}) after subtracting the as-deposited sample spectrum from those of the aged samples. No changes beyond noise can be seen even in the low-energy IR range which is sensitive to chemical variations. The high stability is supported by the XRR patterns which show only ~1% thickness increase (from 97.0 to 98.1 nm) in nearly one month while the density (critical angle) and the roughness (decay rate of total intensity) stay essentially the same for all storage times.

In the humid atmosphere (80% relative humidity), on the other hand, the Eu-HQA films show minor changes in the fingerprint area (<1300 cm^{-1}) of the IR spectra, see Fig. 6(a) (inset). Assignment of these changes is uncertain due to various overlapping peaks in the low-energy region, but they seem to relate to the cleavage of the Eu-HQA network from the Ar—O—Eu and possibly N—O—Eu bonding species: the growing peak at 1260 cm^{-1} most likely originates from the O—H bending of the HQA precursor molecule while the peaks around 1100 and 800 cm^{-1} comprise of the C—N stretching and N—H bending, respectively.[43,44] Regardless, the Eu-HQA films show significant stability even in the humid conditions—especially compared to the most commonly studied, so-called metalcone (e.g., alucone, zincone) films based on aliphatic or aromatic diols as the organic component.[24,45] Interestingly, the present Eu-HQA films have the same M—O—R bonding feature as in the unstable metalcones (suggesting stability issues) but the difference is that our Eu-HQA films contain additionally carboxylate-type M—OO—R bonds which are likely to stabilize the structure. The carboxylate groups are known to form very stable metal-organic compositions.[46,47] Moreover, the large and relative polarizable Eu^{3+} ions (hard acid) bond strongly with the small, nonpolarizable atoms like O and N (hard bases) which should result in a stable complex.

The subtraction plots in Fig. 6(a) inset show that the rate of the composition change decreases with increasing storage time which indicates that a spontaneous passivation layer is formed on the film and the minor decomposition of Eu-HQA occurs mainly at the film surface due to the exposure to the humid air. This assumption is supported by Fig. 6(b) where the main features (critical angle: density, oscillation frequency: film thickness) of the XRR patterns of the 50 nm Eu-HQA film stay similar denoting that the bulk phase of the materials does not change. On the other hand, for the 21-day and 77-day samples, a clear dual-layer structure can be observed which strongly indicates that a second material layer is formed on top of the Eu-HQA film. This oxidized layer is the decomposition product of the Eu-HQA film which is likely to act as a passivation layer and thus protects the low-density Eu-HQA film from further decomposition through preventing infiltration of water vapor.[48]

The minor decomposition in humid environment can be prevented through the capping-layer approach. As seen in Fig. 6(c),

04 April 2025 08:29:42

© Author(s) 2025

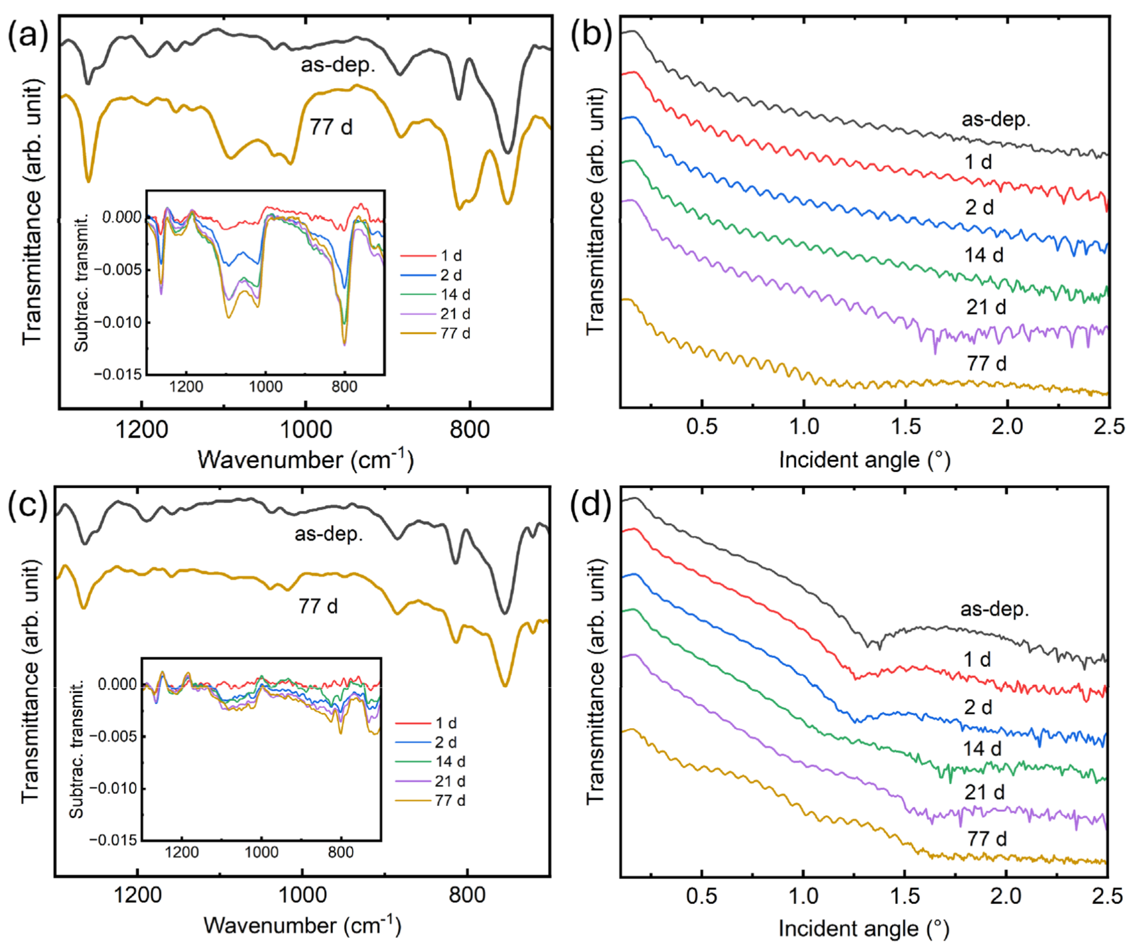

FIG. 6. FTIR spectra and XRR patterns for (a) and (b) Eu-HQA (50 nm) film and (c) and (d) Eu-HQA (50 nm)/Y_2O_3 (4 nm) dual-layer films with indicated storage times in humid air (80% relative humidity at 22 °C). The insets in (a) and (c) show the residual plots after subtracting the as-deposited sample spectrum from the aged samples with indicated storage times.

04 April 2025 08:29:42

the IR spectra of the as-deposited and 77-day-old Eu-HQA/Y_2O_3 film are almost identical which suggests that the Eu-HQA film composition stays intact. The subtraction plots in Fig. 6(c) inset also show negligible changes compared to the Fig. 6(a) inset where capping layer was not employed. However, similar to the single-layer Eu-HQA film [Fig. 6(b)], the dual-layer film gains another top layer during the ageing period [Fig. 6(d)]. As no changes can be observed in the IR spectra, we assign this to a thin H_2O layer; rare-earth metal oxides, including Y_2O_3, have a high tendency for water vapor adsorption.[49] We examined this assumption through XRR simulations and achieved proper fitting for the aged sample only through adding a 2.5 nm H_2O layer on top of the Y_2O_3 capping layer (not shown).

The main drawback of the Eu-HQA thin films in applications such as the FRET-based bioimaging involving direct contact with aqueous solutions is the nearly immediate decomposition/dissolution of the film. Here, we investigated the stability of our Y_2O_3-capped Eu-HQA films in liquid water to study whether the encapsulation improves the film stability in a liquid solution as well. Figure 7 shows the time for decomposition (dissolution) for Eu-HQA (20 nm) films with different Y_2O_3 capping layer thicknesses. Pure Eu-HQA is instantly dissolved in water but then the decomposition time starts to increase with increasing Y_2O_3 capping-layer thickness. With a 4 nm-thick Y_2O_3 capping layer, the dual-layer film starts to visibly dissolve only after 40 s, which is a significant improvement in the stability. Furthermore, increasing the Y_2O_3 layer thickness above the 4 nm seems to greatly enhance the encapsulation effect (Fig. 7). We tentatively assign this to a formation of a more continuous Y_2O_3 capping layer which would prohibit more efficiently the penetration of H_2O through the oxide layer. The 12 nm-thick Y_2O_3 layer might be too thick, e.g., for the FRET-based imaging since minimal distance between the active (Eu-HQA) surface and the fluorescent solution is required for an efficient FRET effect.[29] However, applications without similar restrictions, such as

© Author(s) 2025

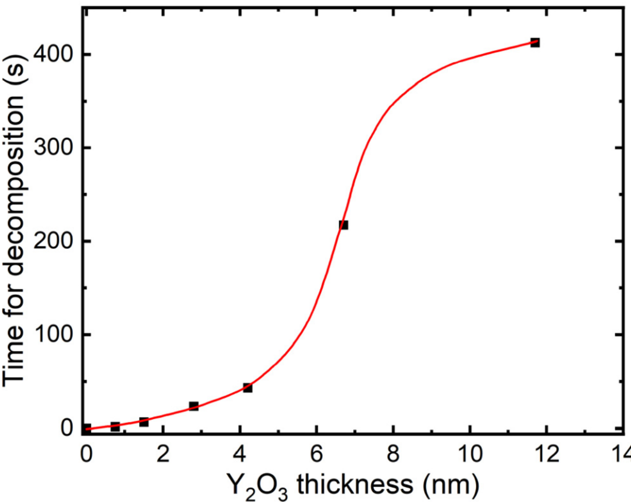

FIG. 7. Stability of the Eu-HQA (20 nm)/Y_2O_3 (x nm) thin films in liquid water. The time for decomposition indicates the time when the luminescence emission disappeared, and the film dissolved after a water droplet was placed on the sample surface. The red line is a guide for the observed trend.

optical thermometry,[50] could benefit from the thicker capping layer and, thus, higher stability as well.

We performed heating tests in air to study the feasible temperature range which could be employed for the cap-less or capped Eu-HQA films (supplementary material). The results show the impressive thermal stability of the single-layer Eu-HQA film up to 340 °C while an 8 nm-thick Y_2O_3 capping could even further improve the stability. It is interesting to note that the thermal stability of Eu-HQA is similar to that of Fe-BDC (BDC = benzene-1,4-dicarboxylic acid) thin films;[46] ALD/MLD-grown materials based on carboxylic acids are typically significantly more stable than those grown from OH- and/or NH_2-based precursors. The present precursor possesses both COOH and NH/OH groups. Hence, it seems that just one COOH group is enough to stabilize the material as observed also from the Eu-HQA aging tests (Fig. 5). This conclusion is important regarding the new ALD/MLD process development, as the acid groups—while improving the stability of the deposition product—unfortunately decrease vapor pressure/increase sublimation temperature (in contrary to, e.g., NH, OH, and SH groups) of organic precursors which strongly limits the applicable deposition temperature range in ALD/MLD. Hence, the combination of acid and secondary reactive groups might be an effective way to balance between the film stability and the precursor volatility.

IV. SUMMARY AND CONCLUSIONS

Here, we demonstrated the *in situ* Y_2O_3 encapsulation of the red luminescent Eu-HQA thin films fabricated via the ALD/MLD + ALD techniques to improve the chemical stability of the Eu-HQA films. The structure, composition, and morphology of the dual-layer films were evaluated using the XRR technique. Both the qualitative observations and quantitative simulations showed the successful deposition of the Eu-HQA/Y_2O_3 dual-layer films with precise control over the Y_2O_3 capping-layer thickness. Minor etching (~2 nm) of the Eu-HQA films was observed due to the strong oxidizing agent (ozone) employed for the Y_2O_3 deposition but it had no significant effect on the composition or luminescence of the films. This illustrates that even O_3 can be utilized in the encapsulation process of metal-organic films if minor surface damage is tolerated. If needed, the etching effect could be most likely avoided by selecting a more reactive yttrium precursor which does not require O_3 as the coreactant. On the other hand, the Y_2O_3 capping-layer decreased the luminescence emission intensity of the Eu-HQA/Ydual-layer films. We believe this issue could be solved by Eu doping of the capping layer to increase the total emission intensity.

The present stability studies show that the single-layer Eu-HQA thin films are appreciably stable in dry air (20% humidity) and show only minor changes in composition in humid atmosphere (80% humidity) over several weeks of storage. These chemical changes could be effectively mitigated by the Y_2O_3 capping layer. In liquid water, the single-layer Eu-HQA is dissolved instantly but, most notably, already an ultrathin (3–4 nm) Y_2O_3 capping layer significantly improved the stability. This is vital for the Eu-HQA films for the FRET bioimaging application. Moreover, the stability tests performed in the dry and humid atmosphere show that even relatively stable ALD/MLD metal-organic films, such as the present Eu-HQA films, can be sensitive to the changing humidity level in air and would likely require encapsulation for applications operating in ambient conditions. Thus developing similar, robust, *in situ* ALD/MLD + ALD capping processes for a broader range of materials is critical for stable device operations.

04 April 2025 08:29:42

SUPPLEMENTARY MATERIAL

See the supplementary material for AFM images of the as-deposited thin films, and FTIR spectra and pictures of the thin-film samples heated at 80–450 °C in air.

ACKNOWLEDGMENTS

Funding was received from the European Union (ERC AdG, UniEnMLD, No. 101097815). Views and opinions expressed are however those of the authors only and do not necessarily reflect those of the European Union or the European Research Council. Neither the European Union nor the granting authority can be held responsible for them. Part of the research was performed at the Micronova Nanofabrication Centre of Aalto University. We thank Dr. Anish Philip for the help with the AFM measurements.

AUTHOR DECLARATIONS

Conflict of Interest

The authors have no conflicts to disclose.

Author Contributions

Topias Jussila: Conceptualization (equal); Formal analysis (lead); Methodology (equal); Writing – original draft (lead); Writing – review & editing (equal). **Joona Pekkanen:** Formal analysis (supporting); Methodology (equal); Writing – review & editing (equal). **Anni Virta:** Formal analysis (equal); Writing – original draft

© Author(s) 2025

(supporting). **Amr Ghazy:** Conceptualization (equal); Methodology (equal); Writing – review & editing (equal). **Mika Lastusaari:** Methodology (equal); Writing – review & editing (supporting). **Maarit Karppinen:** Conceptualization (equal); Funding acquisition (lead); Supervision (lead); Writing – review & editing (lead).

DATA AVAILABILITY

The data that support the findings of this study are available from the corresponding author upon reasonable request.

REFERENCES

[1]J. Zhao, Y. Zhang, Y. Luo, W. Zheng, X. Xu, and F. Luo, Chem. Eng. J. **492**, 152295 (2024).
[2]Y. Liu, Z. Zhao, M. Li, and Z. Zhao, J. Mater. Chem. C **12**, 3394 (2024).
[3]A. Ghazy, M. Lastusaari, and M. Karppinen, Chem. Mater. **35**, 5988 (2023).
[4]M. Rogowska, E. Bruzell, H. Valen, and O. Nilsen, RSC Adv. **12**, 15718 (2022).
[5]J. Smets *et al.*, Chem. Mater. **35**, 1684 (2023).
[6]D. Choudhury, G. Rajaraman, and S. K. Sarkar, RSC Adv. **5**, 29947 (2015).
[7]C. Crivello, S. Sevim, O. Graniel, C. Franco, S. Pané, J. Puigmartí-Luis, and D. Muñoz-Rojas, Mater. Horiz. **8**, 168 (2021).
[8]J. Multia and M. Karppinen, Adv. Mater. Interfaces **9**, 2200210 (2022).
[9]Z. Chai, Y. Liu, J. Li, X. Lu, and D. He, RSC Adv. **4**, 50503 (2014).
[10]A. Ghazy, J. Ylönen, N. Subramaniyam, and M. Karppinen, Nanoscale **15**, 15865 (2023).
[11]M. Heikkinen, R. Ghiyasi, and M. Karppinen, "Layer-engineered functional multilayer thin-film structures and interfaces through atomic and molecular layer deposition," Adv. Mater. Interfaces (published online 2024).
[12]A. P. Ghosh, L. J. Gerenser, C. M. Jarman, and J. E. Fornalik, Appl. Phys. Lett. **86**, 223503 (2005).
[13]J.-S. Park, H. Chae, H. K. Chung, and S. I. Lee, Semicond. Sci. Technol. **26**, 034001 (2011).
[14]B. Wegler, O. Schmidt, and B. Hensel, J. Vac. Sci. Technol. A **33**, 01A147 (2014).
[15]H. Park, S. Shin, H. Choi, N. Lee, Y. Choi, K. Kim, and H. Jeon, J. Vac. Scie. Technol. A **38**, 062403 (2020).
[16]H. Zheng, R. Tian, X. Lu, X. Zhou, J. Chen, X. Liu, and Y. Zhou, Org. Electron. **128**, 107035 (2024).
[17]S. Sarkar, J. H. Culp, J. T. Whyland, M. Garvan, and V. Misra, Org. Electron. **11**, 1896 (2010).
[18]W. J. Potscavage, S. Yoo, B. Domercq, and B. Kippelen, Appl. Phys. Lett. **90**, 253511 (2007).
[19]S. Ferrari, F. Perissinotti, E. Peron, L. Fumagalli, D. Natali, and M. Sampietro, Org. Electron. **8**, 407 (2007).
[20]J. Oh, S. Shin, J. Park, G. Ham, and H. Jeon, Thin Solid Films **599**, 119 (2016).
[21]L. H. Kim *et al.*, Org. Electron. **50**, 296 (2017).
[22]C. Li, M. Cauwe, Y. Yang, D. Schaubroeck, L. Mader, and M. Op de Beeck, Coatings **9**, 579 (2019).
[23]D.-w. Choi, M. Yoo, H. M. Lee, J. Park, H. Y. Kim, and J.-S. Park, ACS Appl. Mater. Interfaces **8**, 12263 (2016).
[24]L. Ghazaryan, E.-B. Kley, A. Tünnermann, and A. Viorica Szeghalmi, J. Vac. Sci. Technol. A **31**, 01A149 (2012).
[25]B. H. Lee, B. Yoon, V. R. Anderson, and S. M. George, J. Phys. Chem. C **116**, 3250 (2012).
[26]G. Chen, Y. Weng, F. Sun, X. Zhou, C. Wu, Q. Yan, T. Guo, and Y. Zhang, RSC Adv. **9**, 20884 (2019).
[27]S. Feng-Bo, D. Yu, Y. Yong-Qiang, C. Ping, D. Ya-Hui, W. Xiao, Y. Dan, and X. Kai-wen, Org. Electron. **15**, 2546 (2014).
[28]Z. Wang, H. Lu, Y. Zhang, C. Liu, H. Zhang, and Y. Yu, Micromachines **15**, 41 (2024).
[29]R. M. Clegg, Curr. Opin. Biotechnol. **6**, 103 (1995).
[30]J. Rosa, M. J. Heikkilä, M. Sirkiä, and S. Merdes, Materials **14**, 1505 (2021).
[31]M. Safdar, A. Ghazy, M. Tuomisto, M. Lastusaari, and M. Karppinen, J. Mater. Sci. **56**, 12634 (2021).
[32]K. J. Eisentraut and R. E. Sievers, J. Am. Chem. Soc. **87**, 5254 (1965).
[33]M. Putkonen, T. Sajavaara, L. S. Johansson, and L. Niinistö, Chem. Vap. Deposition **7**, 44 (2001).
[34]L. Mai, Z. Giedraityte, M. Schmidt, D. Rogalla, S. Scholz, A. D. Wieck, A. Devi, and M. Karppinen, J. Mater. Sci. **52**, 6216 (2017).
[35]A. Ghazy, M. Safdar, M. Lastusaari, and M. Karppinen, Chem. Commun. **56**, 241 (2020).
[36]K. B. Lausund and O. Nilsen, Nat. Commun. **7**, 13578 (2016).
[37]M. Rogowska, P.-A. Hansen, H. H. Sønsteby, J. Dziadkowiec, H. Valen, and O. Nilsen, Dalton Trans. **50**, 12896 (2021).
[38]A. Philip, T. Jussila, J. Obenlüneschloß, D. Zanders, F. Preischel, J. Kinnunen, A. Devi, and M. Karppinen, Small **20**, 2402608 (2024).
[39]N. Boysen, D. Zanders, T. Berning, S. M. J. Beer, D. Rogalla, C. Bock, and A. Devi, RSC Adv. **11**, 2565 (2021).
[40]Y. Etinger-Geller, A. Katsman, and B. Pokroy, Chem. Mater. **29**, 4912 (2017).
[41]H. Jain and P. Poodt, Dalton Trans. **50**, 5807 (2021).
[42]A. Ghazy, D. Zanders, A. Devi, and M. Karppinen, "Atomic and molecular layer deposition of functional thin films based on rare Earth elements," Adv. Mater. Interfaces (published online 2024).
[43]J. E. Stewart, J. Chem. Phys. **30**, 1259 (1959).
[44]J. Coates, "Interpretation of infrared spectra, A practical approach," in *Encyclopedia of Analytical Chemistry*, edited by R. A. Meyers and M. L. McKelvy (Wiley, Chichester, 2006).
[45]Q. Peng, B. Gong, R. M. VanGundy, and G. N. Parsons, Chem. Mater. **21**, 820 (2009).
[46]T. Jussila *et al.*, Chem. Mater. **36**, 6489 (2024).
[47]E. Ahvenniemi and M. Karppinen, Dalton Trans. **45**, 10730 (2016).
[48]M. Aghaee, J.-P. Niemelä, W. M. M. Kessels, and M. Creatore, Dalton Trans. **48**, 3496 (2019).
[49]Y. Kuroda, H. Hamano, T. Mori, Y. Yoshikawa, and M. Nagao, Langmuir **16**, 6937 (2000).
[50]M. N. Getz, O. Nilsen, and P.-A. Hansen, Sci. Rep. **9**, 10247 (2019).

04 April 2025 08:29:42

© Author(s) 2025